Viability and Properties of Roll-to-Roll Coating of Cellulose Nanofibrils on Recycled Paperboard

Vegar Ottesen, Vinay Kumar, Martti Toivakka, Gary Chinga-Carrasco, Kristin Syverud, Øyvind Weiby Gregersen

SUMMARY: Cellulose nanofibrils (CNF) are, due in large part to excellent gas barrier properties, a potential environmentally friendly alternative to inorganic and petrochemical coatings of e.g. paperboard in packaging applications. In the current paper successful roll-to-roll coating of three qualities of CNF is demonstrated on a recycled quality, porous paperboard using a custom-built pilot machine. Single layers of three different thicknesses were applied for each coating. The three CNF qualities used were carboxymethylated CNF (CNF-C), TEMPO-oxidized CNF (CNF-T) and mechanically produced CNF without chemical pre-treatment (CNF-M). All three qualities, which have a range of surface charge, fibril size and fibril size distribution, are shown to produce films that adhere well to the base board. It is revealed that the coating is suspended across surface pores in the base board, as opposed to penetrate into the base board pore structure. Samples were investigated for air and water permeability, gloss, surface roughness and hole density in the coating. Chemically pretreated qualities outperform CNF-M. Addition of 5 wt% carboxy-methyl cellulose (CMC) was shown to reduce hole formation, improve gloss and reduce surface roughness. For thick applications of pre-treated CNF, in particular CNF-C, mechanical strength of the board in and out of the plane increase beyond the un-treated or water treated base board. Possibly a consequence of matter migrating through the base board from the CNF suspension.

ADDRESSES OF THE AUTHORS:

Vegar Ottesen (vegar.ottesen@ntnu.no), Norwegian University of Science and Technology (NTNU), Trondheim, Norway

Vinay Kumar (vinay.kumar@abo.fi), Åbo Akademi University, 20500 Åbo, Finland

Martti Toivakka (Martti.Toivakka@abo.fi), Åbo Akademi University, 20500 Åbo, Finland

Gary Chinga-Carrasco (gary.chinga.carrasco@pfi.no), Paper and Fibre Research Institute (PFI), Trondheim, Norway

Kristin Syverud (kristin.syverud@pfi.no) Norwegian University of Science and Technology (NTNU) and Paper and Fibre Research Institute (PFI), Trondheim, Norway

Øyvind W. Gregersen (oyvind.w.gregersen@ntnu.no) Norwegian University of Science and Technology (NTNU), Trondheim, Norway

Corresponding author: Øyvind Weiby Gregersen

Cellulose nanofibrils (CNF), first produced by homogenization by Turbak and Snyder, is an exciting material that holds significant potential as a key enabling technology in the emerging bioeconomy (Turbak et al. 1983). CNF is a strong material which possesses shear-thinning rheology and is by nature non-toxic, biocompatible and biodegradable. CNF has a wide range of current or potential applications, including, but not limited to, biomedical (Lin, Dufresne 2014; Nordli et al. 2016), electronics (Chinga-Carrasco et al. 2012; Hu et al. 2013; Zheng et al. 2013), cosmetics (Cowie et al. 2014), construction (Peters et al. 2010), and papermaking industries (Lindstrom et al. 2015).

As society transits to a post-petroleum economy, alternatives to current oil-based products are needed. CNF can deliver as a replacement for several inorganic or oil-based products. Among product ranges where CNF may in part or completely replace currently dominating petroleum-based products, we find coatings of a wide range of substrates ranging from paper or board to fabrics in packaging applications (Hamada, Mitsuhashi 2016; Kinnunen et al. 2013; Kumar et al. 2016; Lavoine et al. 2014b; a; Syverud, Stenius 2008), for example aluminum in liquid board in e.g. juice cartons or plastic foil in e.g. cereal bags. CNF coatings are known to impart several beneficial properties to the coated material, e.g. decrease linting (Song, Ankerfors 2010), increase smoothness and significantly decrease permeability for gas and liquids (Aulin et al. 2010; Syverud et al. 2009; Syverud, Stenius 2008).

While plastics and, to some extent, aluminum dominate the barrier coating market today, CNF films offer excellent properties on par with or exceeding those of commercially available polymeric materials (Aulin et al. 2010; Syverud, Stenius 2008). Given the material's properties it has sparked sufficient interest in recent years to be the focus of a significant body of research, as evidenced by several thorough review articles (Aulin, Lindström 2011; Brodin et al. 2014; Lavoine et al. 2012; Lindstrom et al. 2015; Paunonen 2013).

CNF coatings may impart beneficial properties to a substrate such as paper, board or fabrics. Several publications exist describing the properties of CNF as a standalone film or as a coating, of which there is to the authors' best knowledge only one demonstrating roll-to-roll coating (Kumar et al. 2016). Highly fibrillated CNF, such as the qualities used in the current work, typically forms dense but brittle films, which may not survive the coating treatment itself. Moreover, highly fibrillated and charged CNF, such as TEMPO-oxidised CNF (CNF-T) or carboxymethylated CNF (CNF-C), are also very viscous, easily gelating at concentrations well below 1 wt%. The high viscosity presents a challenge in coating applications. Furthermore, to the authors' best knowledge no work has at the current time been done to compare oxidized and mechanically produced CNF in coating applications. The current study addresses the lack of comparisons and descriptive work on different CNF qualities as well as attempting to address the viability of, and describe the

performance of, the CNF qualities in a roll-to-roll coating scenario.

Materials and Methods

Where possible, characterization was done according to relevant established standards, as listed in Table 1. All scanning electron microscopy (SEM) image analysis was performed using FIJI (Schindelin et al. 2012). Atomic force microscopy (AFM) image analysis was performed using Gwyddion (Nečas, Klapetek 2012). Linear regression performed using the statistical software "R" with built-in functionality (Ginestet 2011; R Core Team 2015).

Table 1 – Standards used in current work.

	Standard
Sample Conditioning	ISO 187:1900
Dry matter	ISO 638:178
Air permeance (Gurley)	ISO 5636-5:2013
Tensile properties	ISO 1924-3:2005
Z-strength	Tappi T 541
Gloss	SCAN-P 80
WVTR	ASTM E96/E96M-05

Nanocellulose Production

To investigate the differences between CNF qualities, we prepared three qualities of highly dilute (~0.85 wt%) CNF; CNF-C, CNF-T and CNF-M. CNF-M was prepared from Claflin ground (1 MWh tonne^{-1}) softwood kraft pulp. The pulp was run five passes through a Rannie 15 type 12.56x homogenizer. CNF-T was prepared using two passes, and CNF-C was prepared using three passes. In all cases the first pass was at 600 bar pressure drop while all subsequent passes were run at 1 kbar pressure drop. After fibrillation, each of the three produced qualities were divided into two separate volumes, one without further modification and one which received an addition of 5 wt% Na carboxymethylcellulose (CMC). The CMC used was CP Kelco FINNIFIX$^{®}$ 4000G.

CNF-T was prepared by 2,2,6,6-tetramethylpiperidine-1-oxyl (TEMPO)-oxidation according to Saito et al. (Saito et al. 2007). 2.35 mmol g^{-1} ClO^{-} was used in the TEMPO process. CNF-C was prepared by carboxymethylation according to Wågberg et al. (Wågberg et al. 1987, 2008). In both cases, bleached sulfite was used.

Characterization of Fibrillated Materials

Fibril diameter was measured using transmission electron microscopy (TEM) and AFM. TEM imaging was done using a JEM-1400 Plus TEM using 80 kV acceleration voltage. TEM samples were prepared by drop casting of 0.05 wt% CNF suspension on formvar/carbon-coated 400 mesh copper grids and negatively stained with 1 % (w/v) uranyl acetate in water for 60 s. AFM samples were prepared by drop casting of 0.02 wt% CNF suspension, on freshly cleaved mica discs (F7013 Agar Scientific) and dried by heating on a 65°C hotplate. To avoid tip-sample convolution, fibril diameters were estimated from AFM results using their height. To avoid over-estimation due to fibrils suspended above the mica surface, areas of measurement were only chosen if they were a sufficient distance from points where fibrils meet, cross or split. A Veeco Multimode V AFM using ScanAsyst Air AFM tips was used in tapping mode. Only individualised fibrils were measured, bundles, flocs and fiber fragments were not measured.

Charge of the produced CNF qualities was determined by conductometric titration, as described by Saito and Isogai (Saito, Isogai 2004).

Coating of Base Board

The base board used in the current work was delivered by Dong Il Paper, Korea. The board is a porous, recycled quality paperboard. Cobb-60 value for base board is 255 ± 8 g m^{-2}, and PPS surface roughness is 7.39 ± 0.51 μm. Coated samples were prepared from all prepared CNF qualities, both with and without 5 wt% added CMC. The coating process has been reported elsewhere in more detail (Kumar et al. 2016). Briefly, a custom-built slot die (slot width, 74 mm; slot length, 34 mm; slot gap, 1000 μm) housed on an adjustable rail installed parallel to the axis of a backing roll was used as coating applicator. The distance between the slot die and the substrate referred to as Slot-Web gap can be controlled precisely by the rail movement perpendicular to the backing roll, which enables the slot die to be used as a metering device to control the coating thickness.

CNF with and without added CMC was applied to the base board with three slot-web gaps; 200, 400 and 600 μm. Given that CNF suspensions consist primarily of water; samples were also prepared by using water as opposed to CNF suspension in the coating process. Untreated and water treated base board were also included as a second control. All boards, coated and uncoated, were calendered with a laboratory soft nip calender using a line load of 100 kNm^{-1} and a temperature of 60°C. The samples' back was kept toward the soft roll. The calendering equipment and parameters were the same as used by Kumar et al. (Kumar et al. 2016).

Characterization of Coated Samples

Coating barrier quality was assessed using air resistance (ISO 5636-5:2013) and water vapor transfer rate (WVTR). Low resolution SEM images were recorded to perform both qualitative and quantitative analysis of perforations in the coating. SEM samples were sputter coated with a 4 nm thick PtPd alloy coating and studied in a Hitachi SU4400 SEM using 5 kV acceleration voltage and a 30.5 mm working distance.

Holes in the applied coating were found using FIJI. We defined a hole as any area with a pixel intensity value at or below $\mu - 2\sigma$ for a given image. Thresholding was performed after brightness and contrast correction and a noise reduction using FIJI's built-in "remove salt-and-pepper" function. From binarized images, holes were measured and quantified using the "Shape Descriptor" ImageJ/FIJI plugin described by Syverud et al. (Syverud et al. 2007).

Coating smoothness was characterized by gloss and mean facet polar orientation (FPO) measured in degrees. As a function of surface roughness (Chinga-Carrasco et al.

2008), FPO correlates with, and describes the topographical contribution to, gloss.

Adhesion between coating and base board and coating thickness was further assessed by both Z-strength measurements and SEM investigations of cross-sections. Cross-sections were prepared by two methods; ion milling or epoxy embedding with subsequent grinding and polishing. Epoxy embedding was performed as described by Chinga and Helle (Chinga-Carrasco, Helle 2002). Ion milling of paper samples was performed using a Hitachi IM4000 ion mill. Milling was performed for 14 hours using an acceleration voltage of 3.8 kV. After milling, the sample cross-section was sputter-coated with 5 nm gold. Imaging was performed at 5 kV with a working distance of 7.2 mm. Tensile (ISO 1924-3:2005) and Z-strength (Tappi T 451) were also tested.

Thickness of applied coating is reported as slot-web gap distance. Quantitative coating thickness was evaluated using a rolling ball algorithm applied to thresholded cross-section images. Thresholding was done by first isolating the coating on SEM micrographs of epoxy-embedded cross-section samples, and binarizing the images. A rolling ball algorithm was then applied to the binarized image, as described by Chinga and Helle (Chinga-Carrasco, Helle 2002). Only areas where the film was freely suspended across surface pores or only briefly in contact with underlying support were used. This was done to facilitate identification of the coating layer and minimize mislabeling of the base board as the coating layer. The rolling ball diameter was set to 0.4 μm. Evaluation was performed for samples coated using 400 and 600 μm slot-web gaps only.

Statistical Analysis of Results

Individual factors (e.g. air resistance or holes/mm^2) were tested for normalcy and a multiple linear regression was performed using built-in functionality in the statistical software "R". Resulting models were examined for significance using a Student-t-test included in the lm function (R Core Team 2015). Multiple linear regression models were made using holes per mm^2, air resistance, roughness (Rq) and z-strength as responses. CNF quality, added CMC (0 or 5 wt%) and slot-web gap (200, 400 or 600 μm) were used as predictors in the generated models.

Results and Discussion

CNF Quality, Fibrillation and Fibril Diameter

To measure the diameter of produced nanofibrils we used atomic force microscopy (AFM) and transmission electron microscopy (TEM). The results, shown in Fig. 1., show that fibril diameter differ between the qualities and that the CNF-M has the largest fibrils by far with a mean diameter above 10 nm, more than twice as large as CNF-T fibrils. While these fibrils are from two different wood pulps, it is worth noting that this should have negligible effect on the experimental outcome. We expect so due to the known

effect of differences in mean fibril diameter and the chemical modifications due to the oxidation pre-treatments (Syverud et al. 2009).
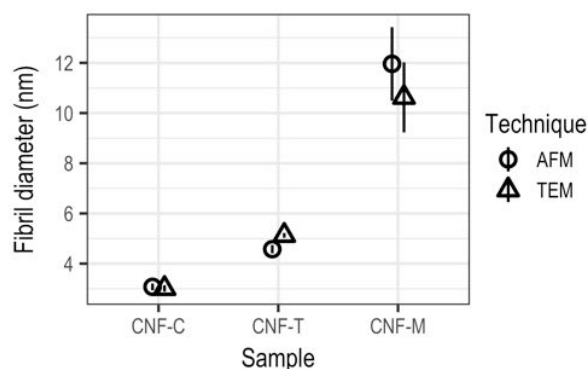

Fig 1 - Diameter of produced nanofibrils in nm measured by AFM and TEM. To avoid tip-sample convolution in AFM analysis was performed using fibril height, as opposed to the fibril width. Error bars denote standard error. Only individual fibrils were measured, not fiber fragments or bundles of fibrils.

Partial dissolution of CNF-C during the pre-treatment step is the likely cause for the features seen in Fig. 2. (a1) and Fig. 3. These figures show what appears to be slopes on the side of the CNF-C nanofibrils, features which are not visible in TEM micrographs. These slopes may have formed during drying by deposition of dissolved or partly dissolved molecules from the fibril suspension. We expect the slopes to be primarily composed of CMC which is either partly associated with the fibrils, or completely dissolved. The observed features may consist of partly dissolved fibrils spread out on the underlying mica surface, or CMC molecules which may have been deposited by the retreating water meniscus. In both cases clustering near other components in the suspension on the mica surface may be a result. The absence of such features for qualities CNF-T and the CNF-M also used may be seen to support this interpretation. Their absence from TEM micrographs may be explained by the lightweight nature of polymeric CMC; resting on the thin carbon film support on top of the TEM grid, these polymers may be indistinguishable from the background.

Table 2 - Charge and charge standard deviation of CNF qualities. Measured by conductometric titration, as described by Saito and Isogai (Saito, Isogai 2004).

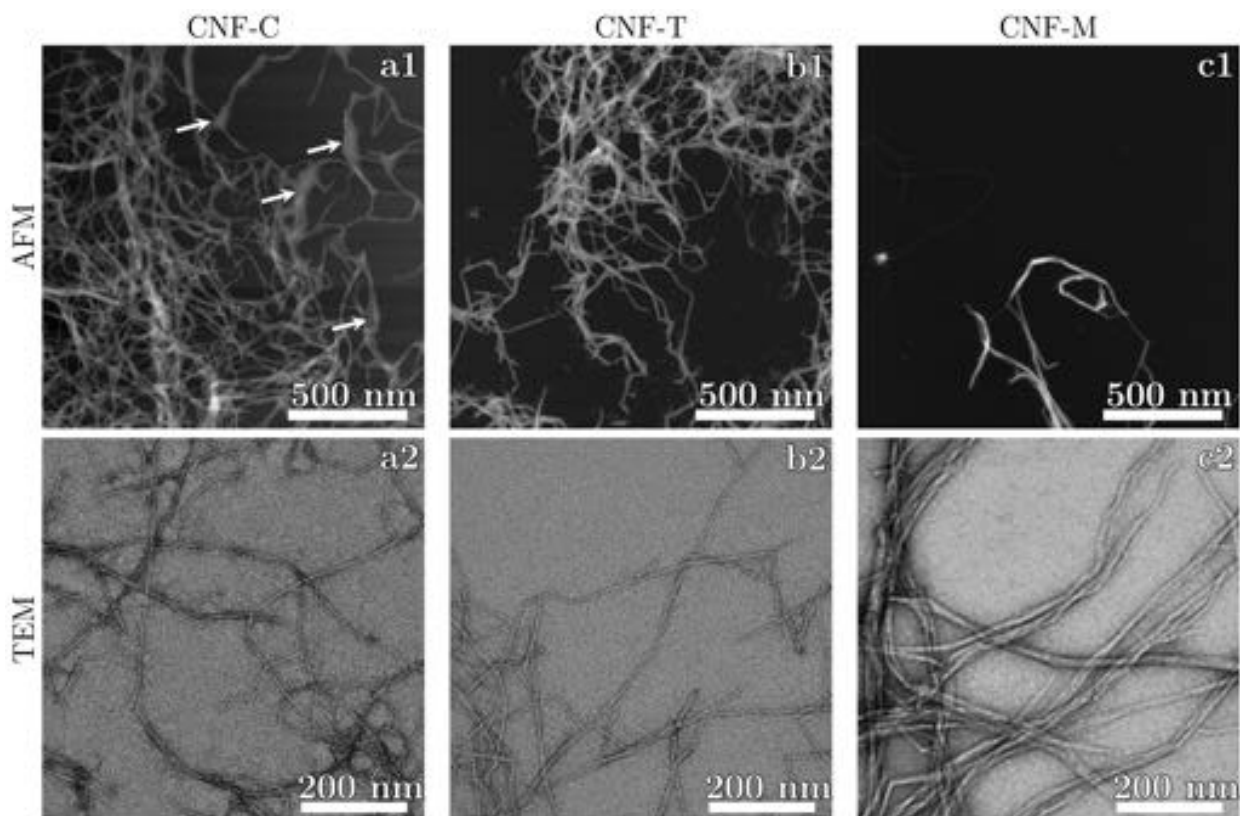|	CNF-C	CNF-T	CNF-M
Charge (μmol g^{-1})	476	910	248
Standard deviation (μmol g^{-1})	63.7	61.2	7.3

Fig. 2. Nanofibrils imaged using AFM (row 1) and TEM (row 2) CNF-C (column a) and CNF-T (column b) and CNF-M (column c). Arrows in b1 point to sloped deposits alongside nanofibrils, possibly formed during drying. Subfigure a1 is repeated in Fig. 3 for emphasis and clarity. AFM micrographs show height information. Black pixels denote 0 nm, white pixels denote 22.9 nm (a1), 20.1 nm (b1) and 18.4 nm (c1).
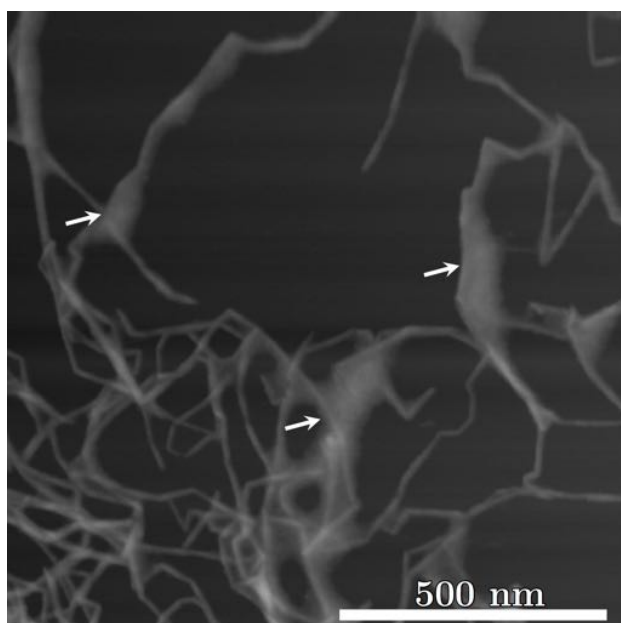

Fig. 3. CNF-C nanofibrils imaged using AFM. Area is extracted from top-right corner of Fig. 2. a1 for emphasis. Arrows point to slopes along sides of nanofibrils.

Coating Integrity

Films cast from pure CNF are known to possess barrier properties equal to or better than the best polymeric materials, even at low grammages (Syverud, Stenius 2008). This excellent barrier ability depends on the film being defect-free, in which case permeability is diffusion-limited. For paper coating it is vital that the applied coating covers the surface of the base board, holes in the coating will reduce or eliminate the desired barrier property.

To investigate the coating quality SEM images of the surface (Fig. 4) were recorded. The SEM micrographs show more apparent holes per unit area for samples coated with CNF-M as compared with CNF-C and CNF-T (Table 3, Figs. 5 and 6).

Significant differences were seen in both average hole area and number of holes per unit area between CNF qualities, though addition of CMC shows no strong statistical significance on either the number of holes per unit area, this is tabulated in Table 3.

The plots in Fig. 5 reveal that transport across CNF coatings of both air and water vapor are heavily dependent on the porosity of the barrier film. However, air permeability seems to be more affected than water vapor transfer rate. This may be explained by solid state diffusion being more important for WVTR as compared to air permeability (Aulin et al. 2010; Minelli et al. 2010). Mean fibril diameter (Fig. 1) can be expected to contribute to hole formation. This is consistent with the information shown in Fig. 5 and is also consistent with significance revealed in Table 3, which shows CNF quality is significantly associated with hole density.

Despite improved barrier properties, coated samples fall short of values reported for self-standing films (Aulin et al.

2010; Syverud, Stenius 2008). Qualitatively, images show that holes frequently appear alongside fibers or structures protruding from the paper surface, consistent with literature (Miettinen et al. 2014). By analyzing the multiple linear regression models we find hole density is strongly correlated with both thickness of applied CNF (slot-web gap) and CNF quality (Table 3). Examining cross sections of the coated paper (Fig. 6), it seems surface pores in the base board are less problematic than protrusions; grooves or surface pores in the board are covered by a film of the deposited CNF.

From Table 3, it is also clear that CMC addition correlates with air resistance - but not hole formation. It seems reasonable to assume a causative relationship; the reason for CMC's positive effect on air permeability may be due to the smaller CMC polymers filling minute gaps in the applied coating, increasing its density and reducing diffusivity for non-polar gases, such as nitrogen and oxygen, primary components of air. Such an effect should increase the air resistance for coatings with few holes per unit area, when mass transport is increasingly dependent on diffusion. Such a dependence is what Fig. 5 shows, in particular for air resistance (Fig. 5 a). The beneficial effect of added CMC may also explain some of the reason why CNF-C produces better air barrier films than CNF-T. While no statistically significant effect of CMC can be shown for number of holes per mm^2, it is significantly correlated with air permeability, as seen from regression lines in Fig. 5.

An analysis of both permeability and SEM images of the surface reveals that the coat integrity depends strongly on the quality of CNF used. Qualitatively, analyzing images of sample cross-sections suggest that all tested qualities manage to form films which can span pores, covering them in a uniform, whole film as seen in Fig. 6. To our knowledge the ability of CNF to form films suspended across pores in the base board surface has not been previously described in peer reviewed literature.
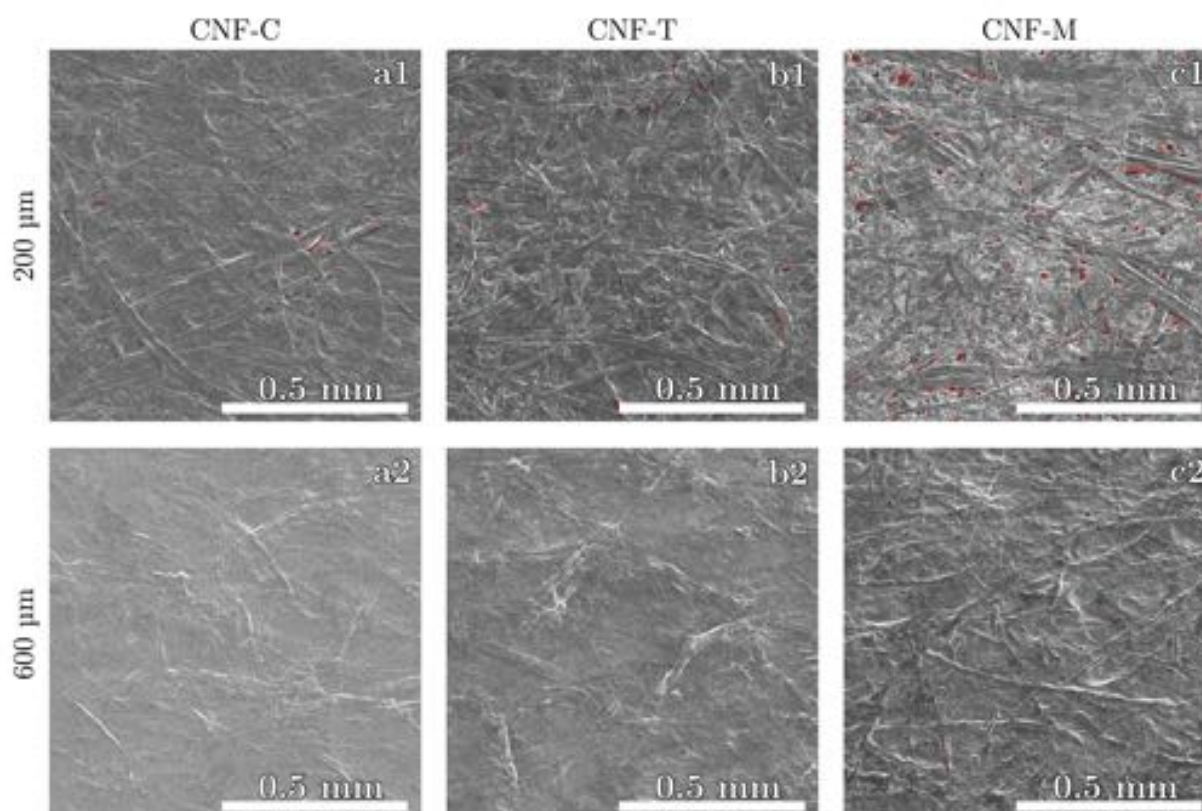

Fig. 4. Thresholded images showing detected pores in red overlayed on SEM micrographs. CNF-C (column a) CNF-T (column b) and CNF-M (column c). Samples coated using slot-web gaps of 200 μm (row 1) and 600 μm (row 2) are shown. Images have been cropped from originals.

Table 3. p-values and adjusted R2 for performed multiple linear regression. Columns show responses while rows are predictors

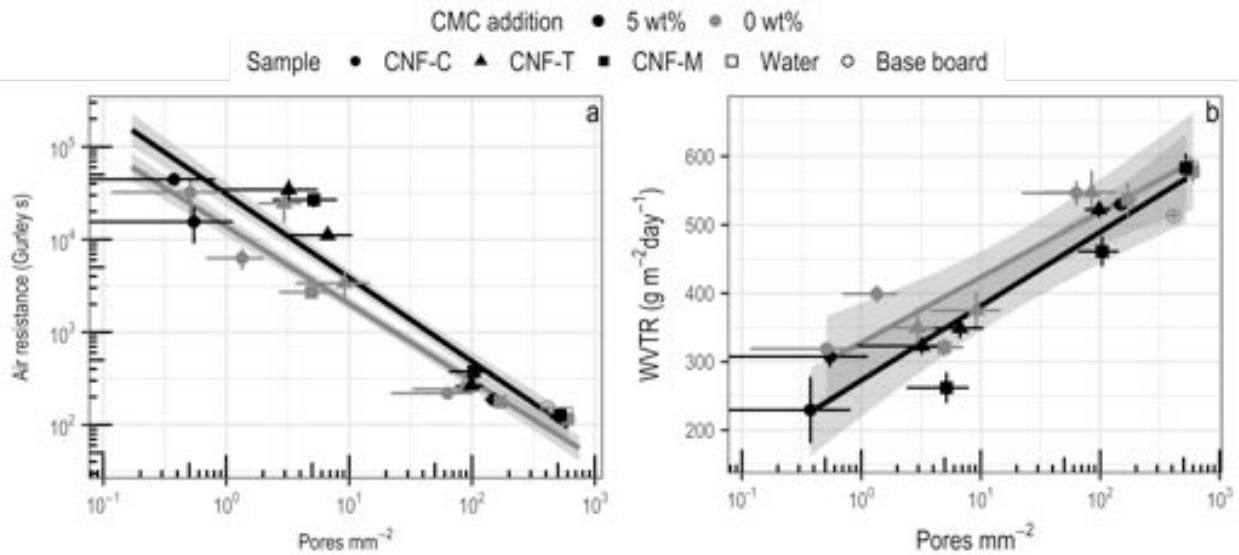| Response	CMC (p-value)	Slot-web gap (p-value)	CNF quality (p-value)	Adjusted R^2
Holes mm^{-2}	0.24	$<2*10^{-16}$	$3.78*10^{-12}$	0.56
Air resistance	$1.06*10^{-7}$	$<2*10^{-16}$	$<2*10^{-16}$	0.70
Roughness (Rq)	0.11	$<2*10^{-16}$	0.00114	0.39
Z-strength	0.46	$<2*10^{-16}$	$3.84*10^{-5}$	0.24

Fig. 5. Air resistance in Gurley s, plotted against pores per mm² (a). Higher Gurley values imply lower permeability, higher resistance. Water Vapor Transfer Rate (WVTR) plotted against pores per mm² (b). Higher WVTR values imply greater permeability. Error bars show standard deviation. Gray area around regression lines show standard error, error bars denote standard deviation. Regression performed separately for samples with and without added CMC.
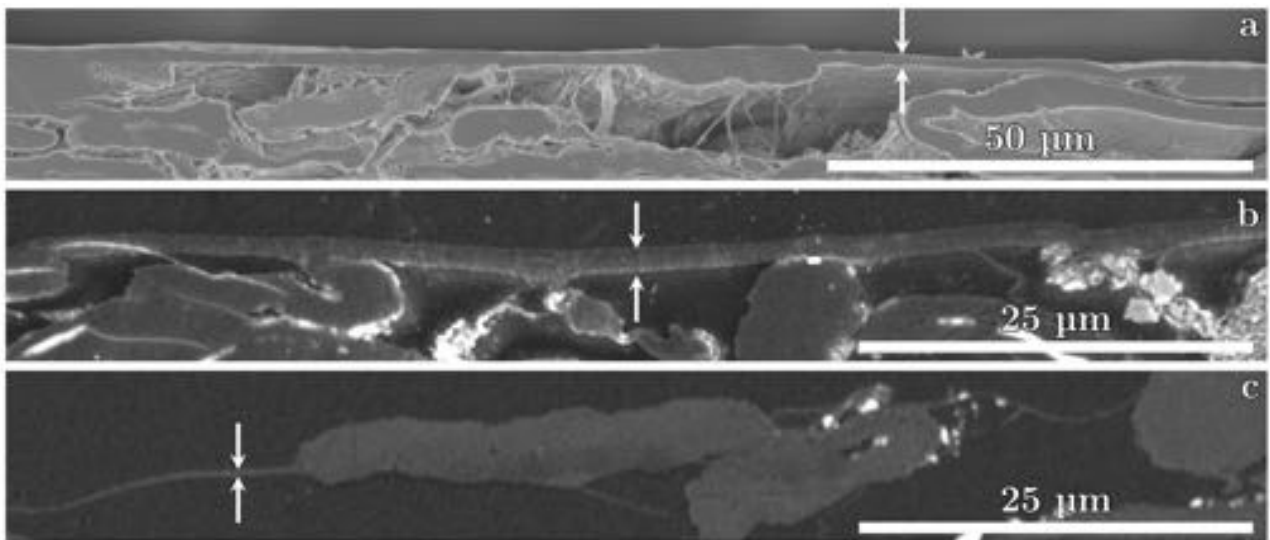

Fig. 6. Cross-sections of CNF-T samples. Slot-web gaps of 600 µm (a), 400 µm (b) and 200 µm (c) are shown. Samples are ion milled and sputter coated with 5 nm gold (a) or epoxy-embedded and carbon-coated as described by Chinga et al. (b, c) (Chinga-Carrasco et al. 2004). Images have been cropped. All images were recorded using 5 kV acceleration voltage and a SE detector. Arrows indicate the CNF-T coating has formed a distinct film bridging surface pores.

Cross-sections of our samples show that the coating can span pores in the substrate while maintaining integrity and thickness in that area. As Fig. 7 reveals, the coating thickness uniformity is dependent on CNF quality. Our thickness measurements reveal that CNF-M produces a less even coat than the other qualities used. This is consistent with roughness parameter Rq as measured by laser profilometry (Fig. 8) and quantitative data from SEM surface images (Figs. 5 and 7), which reveal CNF-M produces a rougher coating with a higher likelihood of hole formation. The source of this may be the higher mean fibril diameter in CNF-M. We believe the formation of a distinct film suspended across pores is a consequence of internal forces within the film during drying. We suspect in particular two major factors contribute to the observed film-forming behavior; surface charge and specific surface area (SSA). As the CNF suspension is applied to the base board, capillary forces will pull the suspension into the base board pore structure. The more viscous the fibril suspension is, the slower this penetration will be, keeping the suspension on the base board surface. Given that both increased SSA and increased surface charge increase viscosity, they can both be expected to reduce permeation of the fibril suspension into the base board. As water is removed during drying, an increasing number of hydrogen bonds will form between fibrils and between fibrils and the base board. Given the high SSA of the fibrils, the clear majority of these formed bonds will be between fibrils, not

between fibrils and the base board. As the coating film dries, its strength increases and swelling decreases, eventually releasing parts of the surface and forming films, as seen in Fig. 6. Note that rod or bladed systems may apply more force pushing the fibril suspension further into the base board than the technique used in the current paper, potentially countering the contribution to film formation from CNF suspension viscosity.
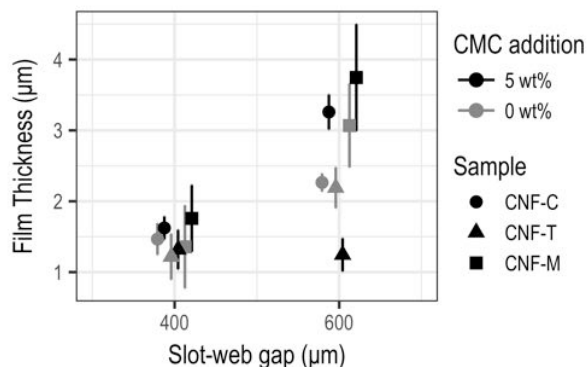

Fig. 7. Coating thickness measured on SEM images of epoxy-embedded cross-sections of the samples. Measurements done using a rolling ball algorithm with a ball diameter of 0.4 μm, as described by Chinga and Helle [33]. Measurements performed for 400 and 600 μm slot-web gaps. Error bars indicate standard deviation.

A highly significant correlation between surface roughness and CNF quality is shown (Table 3) despite noisy data (low R^2). As the data is plotted (Fig. 8) we see that CNF-C and CNF-T reduce the paperboard roughness with increased slot-web gap. The same reduction is not evident for CNF-M. For CNF-C and CNF-T, roughness values were shown to decrease to approximately 1.5 times that of films cast from pure CNF. While films cast from pure CNF-M have low roughness, the quality does not reduce the surface roughness of the base board by a significant degree within the tested range of slot-web gaps.
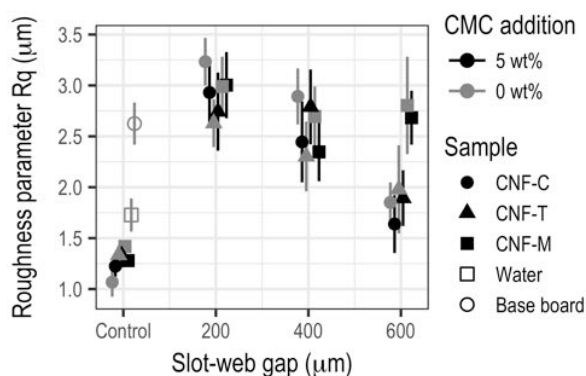

Fig. 8. Roughness (Rq) is plotted against slot-web gap (μm) (c). Control samples include the base board and solvent cast CNF films. Error bars denote standard deviation.

As one may suspect given the above, the ability to form smooth, pore-bridging coatings is shown to correlate with both CNF quality and slot-web gap (Table 3). The impact of CNF quality is likely primarily due to fibril mean diameter. As the mean diameter increases, the number of potential hydrogen bonds between fibrils decreases. It is worth noting that particularly large fibers or fiber fragments will introduce interfaces along which defects may form, increasing hole formation as well. In general, we can say that a weaker film has a higher likelihood of hole formation. Strength can be increased by increasing film thickness, by increasing the slot-web gap, or by increasing the SSA, thereby increasing internal bonding in the film. CNF-M, which has a higher mean fibril diameter, has a reduced ability to bridge surface pores as compared with CNF-T and CNF-C. This reduced ability is clear even at high slot-web gaps (Fig 6), and may likely be due to the higher fibril diameter (Fig. 1).

The ability to cover pores and form an uninterrupted film across gaps in the base board is supported by laser profilometry (Fig. 8). Laser profilometry of solvent cast films of the three tested CNF qualities show only small differences in roughness. This similarity in roughness is not preserved when the different qualities are used as a coating. We can note that Fig. 9 shows that both roughness and FPO follow the same differences we see between CNF-M, CNF-C and CNF-T for other properties tested. CNF-M yields relatively rough surfaces, which decrease the corresponding gloss levels. Hence, CNF-M produces less beneficial results as compared to CNF-C and CNF-T with respect to permeability, likelihood of hole formation in the coating and roughness.
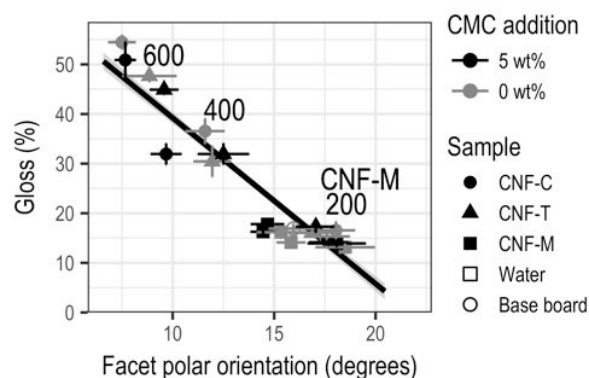

Fig. 9. Gloss values for all samples. FPO is plotted against gloss (%). Slot-web gap is indicated by clusters of points in the plot. Given that all CNF-M points cluster alongside the 200 μm slot-web gap point for CNF-C and CNF-T this is also annotated. The gray zone around the interpolation line is standard error. Error bars denote standard deviation.

Effects of Coating on Mechanical Properties

Coating adhesion to the base board is important for coating integrity and durability; poor adhesion can lead to delamination during the coating process itself, during printing, folding/creasing or other processes involving the coated board. Coating adhesion, therefore, is an important property which can be quantitatively assessed by measuring the z-strength of the coated product. In the event of good adhesion between the coating and base board, this measure can be expected to be unchanged after coating of the substrate; the base board's strength will be the limiting factor, not the interface between base board and coating layer.
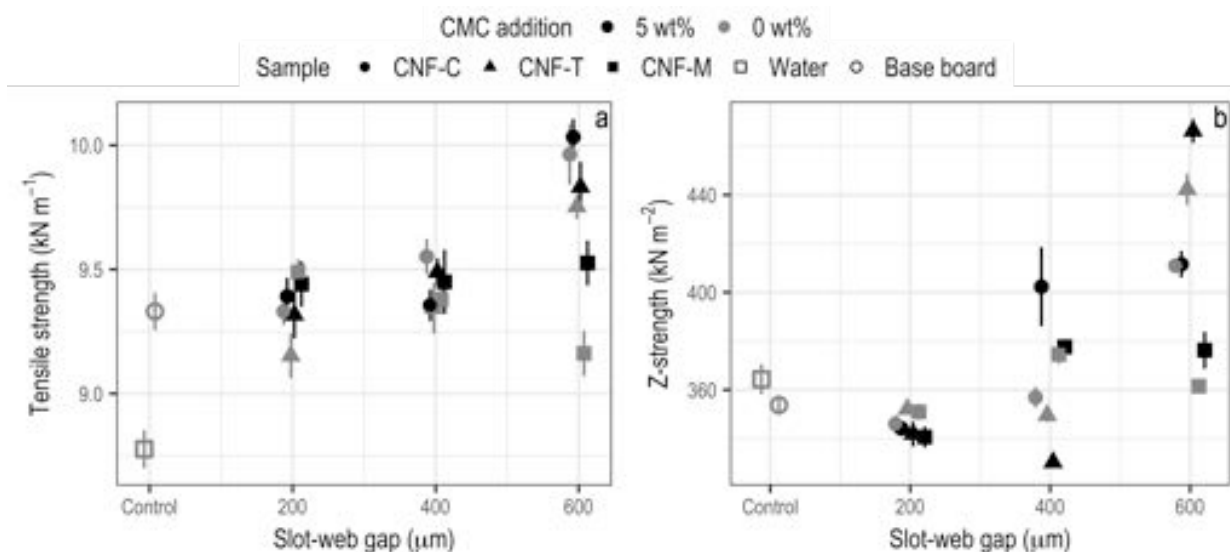
Fig. 10. Tensile strength in kN m^{-1} (a) and Z-strength in kN m^{-2} (b) plotted against slot-web gap in µm. Error bars denote standard error.

While a high z-strength, showing good adhesion, is demonstrated, the observed effect runs contrary to expectations as the z-strength is shown to increase beyond the inherent strength of the base board for larger slot-web gaps (Fig. 10b). As slot-web gap increases, particularly for CNF-C and CNF-T, z-strength increases. A similar effect is also seen for tensile strength (Fig. 10a). The increase relative to the untreated base board shows that the internal bonding in the base board has increased for the thicker applied coatings. Given that the applied CNF coat forms a film suspended over pores (Fig. 6), we can exclude the coating filling the board's pore network as an explanation. Rather, a more likely explanation is that a portion of matter from the applied suspension has migrated independently of the eventual coating, binding paper components more strongly to one another.

Adhesion between a coating layer and the base board is clearly strong in the described case. Adhesion is typically mediated by two main mechanisms: Chemical bonding and mechanical interlocking. Given that the base board used in the current experiment is highly porous and rough, mechanical interlocking may seem a likely candidate. However, cross-sectional examination (Fig. 6) reveals that the coating forms a distinct film, bridging surface pores as opposed to penetrating them. This means that any contribution to coating adhesion from mechanical interlocking is from topography smaller than what is distinguishable in recorded SEM images. A likely conclusion is that the largest contributor to coating adhesion is chemical bonding. In the described case, bonding between the applied coating and the base board will be in the form of numerous hydrogen bonds.

Conclusions

1. Coating of CNF with low solid content is demonstrated. We found that oxidized CNF qualities provide superior coating as compared to CNF-M, likely a result of lower fibril diameter and narrower fibril diameter distribution. Oxidized qualities provided superior barrier properties and higher smoothness than CNF with no chemical pre-treatment. For all CNF qualities, addition of 5 wt% CMC to the CNF suspension improved air barrier properties, likely by increasing the coating density.

2. CNF coats of sufficient thickness do not permeate surface pores, but instead form films suspended across surface pores in the base board. We believe this formation of a distinct film occurs during drying and is attributed to the formation of numerous hydrogen bonds between fibrils in the film, which favors film formation over adhesion to board microtopography. This ability of CNF to form films distinct and separate from the surface initially coated by the CNF suspension prior to drying is likely to be of relevance to other scenaria where CNF is used in conjunction with other materials.

3. Good adhesion between CNF coating and the base board is demonstrated and believed to be caused by chemical adhesion, by way of numerous hydrogen bonds, as opposed to mechanical interlocking between the CNF coating and the base board. This is supported by the CNF coating forming a distinct film suspended on top of the base board as opposed to penetrating base board pore structure. As coating thickness increases the internal strength of the base board is shown to increase beyond the strength of untreated base board for CNF-C and CNF-T. This increase in internal bond strength is likely caused by matter migrating through the base board from the applied fibril suspension.

Acknowledgements

Literature

Aulin, C., Gällstedt, M. and Lindström, T. (2010): Oxygen and oil barrier properties of microfibrillated cellulose films and coatings. Cellulose, 17(3), 559–574.

Aulin, C. and Lindström, T. (2011): Biopolymer Coatings for Paper and Paperboard. Biopolym. - New Mater. Sustain. Film. Coatings, John Wiley & Sons, Ltd, Chichester, UK, 255–276.

Brodin, F. W., Gregersen, Ø. W. and Syverud, K. (2014): Cellulose nanofibrils: Challenges and possibilities as a paper additive or coating material - A review. Nord. Pulp Pap. Res. J., 29(1), 156–166.

Chinga-Carrasco, G. and Helle, T. (2002): Structure characterisation of pigment coating layer on paper by scanning electron microscopy and image analysis. Nord. Pulp Pap. Res. J., 17(3), 307–312.

Chinga-Carrasco, G., Johnsen, P. O. and Diserud, O. (2004): Controlled serial grinding for high-resolution three-dimensional reconstruction. J. Microsc., Blackwell Science Ltd, 214(Pt 1), 13–21.

Chinga-Carrasco, G., Kauko, H., Myllys, M., Timonen, J., Wang, B., Zhou, M. and Fossum, J. O. (2008): New advances in the 3D characterization of mineral coating layers on paper. J. Microsc., 232(2), 212–224.

Chinga-Carrasco, G., Tobjörk, D. and Österbacka, R. (2012): Inkjet-printed silver nanoparticles on nano-engineered cellulose films for electrically conducting structures and organic transistors: concept and challenges. J. Nanoparticle Res., 14(11), 1213.

Cowie, J., Bilek, E. M. T., Wegner, T. H. and Shatkin, J. A. (2014): Market projections of cellulose nanomaterial-enabled products - part 2: Volume estimates. Tappi J., 13(6), 57–69.

Ginestet, C. (2011): ggplot2: Elegant Graphics for Data Analysis. J. R. Stat. Soc. Ser. A (Statistics Soc., 174(1), 245–246.

Hamada, H. and Mitsuhashi, M. (2016): Effect of cellulose nanofibers as a coating agent for woven and nonwoven fabrics. Nord. Pulp Pap. Res. J., 31(2), 255–260.

Hu, L., Zheng, G., Yao, J., Liu, N., Weil, B., Eskilsson, M., Karabulut, E., Ruan, Z., Fan, S., Bloking, J. T., McGehee, M. D., Wågberg, L. and Cui, Y. (2013): Transparent and conductive paper from nanocellulose fibers. Energy Environ. Sci., 6(2), 513–518.

Kinnunen, K., Hjelt, T., Kenttä, E. and Forsström, U. (2013): Thin Coatings for Paper by Foam Coating. Pap. 2013.

Kumar, V., Elfving, A., Koivula, H., Bousfield, D. and Toivakka, M. (2016): Roll-to-Roll Processed Cellulose Nanofiber Coatings. Ind. Eng. Chem. Res., American Chemical Society, 55(12), 3603–3613.

Lavoine, N., Bras, J. and Desloges, I. (2014a): Mechanical and barrier properties of cardboard and 3D packaging coated with microfibrillated cellulose. J. Appl. Polym. Sci., 131(8), n/a-n/a.

Lavoine, N., Desloges, I., Dufresne, A. and Bras, J. (2012): Microfibrillated cellulose - its barrier properties and applications in cellulosic materials: a review. Carbohydr. Polym., Elsevier Ltd., 90(2), 735–64.

Lavoine, N., Desloges, I., Khelifi, B. and Bras, J. (2014b): Impact of different coating processes of microfibrillated cellulose on the mechanical and barrier properties of paper. J. Mater. Sci., 49(7), 2879–2893.

Lin, N. and Dufresne, A. (2014): Nanocellulose in biomedicine: Current status and future prospect. Eur. Polym. J., 59, 302–325.

Lindstrom, T., Naderi, A. and Wiberg, A. (2015): Large Scale Applications of Nanocellulosic Materials - A Comprehensive Review -. J. Korea Tech. Assoc. Pulp Pap. Ind., Korean Technical Assoc. of the Pulp and Paper Industry, 47(6), 5–21.

Miettinen, A., Chinga-Carrasco, G. and Kataja, M. (2014): Three-Dimensional Microstructural Properties of Nanofibrillated Cellulose Films. Int. J. Mol. Sci., 15(4), 6423–6440.

Minelli, M., Baschetti, M. G., Doghieri, F., Ankerfors, M., Lindström, T., Siró, I. and Plackett, D. (2010): Investigation of mass transport properties of microfibrillated cellulose (MFC) films. J. Memb. Sci., 358(1–2), 67–75.

Nečas, D. and Klapetek, P. (2012): Gwyddion: an open-source software for SPM data analysis. Open Phys., 10(1).

Nordli, H. R., Chinga-Carrasco, G., Rokstad, A. M. and Pukstad, B. (2016): Producing ultrapure wood cellulose nanofibrils and evaluating the cytotoxicity using human skin cells. Carbohydr. Polym., 150, 65–73.

Paunonen, S. (2013): Strength and barrier enhancements of composites and packaging boards by nanocelluloses-a literature review. Nord. Pulp Pap. Res. J., 28(Soroka), 165–181.

Peters, S., Rushing, T., Landis, E. and Cummins, T. (2010): Nanocellulose and Microcellulose Fibers for Concrete. Transp. Res. Rec. J. Transp. Res. Board, 2142, 25–28.

R Core Team. (2015): R: A Language and Environment for Statistical Computing. R Found. Stat. Comput. Vienna Austria.

Saito, T. and Isogai, A. (2004): TEMPO-mediated oxidation of native cellulose. The effect of oxidation conditions on chemical and crystal structures of the water-insoluble fractions. Biomacromolecules, 5(5), 1983–1989.

Saito, T., Kimura, S., Nishiyama, Y. and Isogai, A. (2007): Cellulose nanofibers prepared by TEMPO-mediated oxidation of native cellulose. Biomacromolecules, 8(8), 2485–2491.

Schindelin, J., Arganda-Carreras, I., Frise, E., Kaynig, V., Longair, M., Pietzsch, T., Preibisch, S., Rueden, C., Saalfeld, S., Schmid, B., Tinevez, J.-Y., White, D. J., Hartenstein, V., Eliceiri, K., Tomancak, P. and Cardona, A. (2012): Fiji: an open-source platform for biological-image analysis. Nat. Methods, Nature Publishing Group, a division of Macmillan Publishers Limited. All Rights Reserved., 9(7), 676–82.

Song, H. and Ankerfors, M. (2010): Reduction of the linting and

dusting propensity of newspaper using starch and microfibrillated cellulose. Nord. Pulp Pap. Res. J., 25(4), 495–504.

Syverud, K., Chinga, G., Johnsen, P. O., Leirset, I. and Wiik, K. (2007): Analysis of lint particles from full-scale printing trials. Appita J. J. Tech. Assoc. Aust. New Zeal. Pulp Pap. Ind., 60(4), 286–290.

Syverud, K., Gregersen, Ø. W., Chinga-Carrasco, G. and Eriksen, Ø. (2009): The influence of MFC on paper strength and surface properties. Adv. pulp Pap. Res., Pulp and Paper Fundamental Research Society, Oxford, 899–930.

Syverud, K. and Stenius, P. (2008): Strength and barrier properties of MFC films. Cellulose, 16(1), 75–85.

Turbak, A. F., Snyder, F. W., Sandberg, K. R. and A.F. Turbak, F. W. S. (1983): Microfibrillated cellulose, a new cellulose product: properties, uses, and commercial potential. J. Appl. Polym. Sci. Appl. Polym. Symp.; (United States).

Wågberg, L., Decher, G., Norgren, M., Lindström, T., Ankerfors, M. and Axnäs, K. (2008): The build-up of polyelectrolyte multilayers of microfibrillated cellulose and cationic polyelectrolytes. Langmuir, 24(3), 784–95.

Wågberg, L., Winter, L., Ödberg, L. and Lindström, T. (1987): On the charge stoichiometry upon adsorption of a cationic polyelectrolyte on cellulosic materials. Colloids and Surfaces, 27(1–3), 163–173.

Zheng, G., Cui, Y., Karabulut, E., Wågberg, L., Zhu, H. and Hu, L. (2013): Nanostructured paper for flexible energy and electronic devices. MRS Bull., 38(4), 320–325.